Supplementary Information (SI) for Environmental Science: Atmospheres.
This journal is © The Royal Society of Chemistry 2024

O_3 chemistry of 2,5-dimethylfuran: Mechanism development

- Supporting Information -

N. Illmann, and V. Rösgen

Table of Contents

A. Experimental conditions

Table S1 Summary of the conditions of all performed experiments.

Experiment	Target	Instrumentation	Initial mixing ratios/ ppmV	
EXP1	Rate coefficient determination [a]	FTIR, PTR-MS	25DMF: E2B: cHexene:	1.1 1.4 0.5
EXP2	Rate coefficient determination [a]	FTIR, PTR-MS	25DMF: E2B: cHexene:	1.1 1.5 0.6
EXP3	Rate coefficient determination [a]	PTR-MS	25DMF: E2B: cHexene:	0.4 0.7 0.3
EXP4	OH production	FTIR	25DMF: 135TMB:	1.1 0.8
EXP5	OH production	FTIR	25DMF: 135TMB:	1.1 1.6
EXP6	OH production	FTIR	25DMF: 135TMB:	0.9 1.5
EXP7	OH production	PTR-MS, (FTIR)[b]	25DMF: 135TMB:	0.72 1.6
EXP8	OH production	PTR-MS, (FTIR)[b]	25DMF: 135TMB:	1.1 0.61
EXP9	OH production	PTR-MS, (FTIR)[b]	25DMF: 135TMB:	0.89 0.47
EXP10	OH production	PTR-MS, (FTIR)[b]	25DMF: 135TMB:	0.47 1.4
EXP11	OH production	PTR-MS, (FTIR)[b]	25DMF: 135TMB:	0.54 1.1
EXP12	Product formation [a]	FTIR, PTR-MS	25DMF:	1.2
EXP13	Product formation [a]	FTIR, PTR-MS	25DMF:	1.5
EXP14	Product formation [a]	FTIR, PTR-MS	25DMF:	1.1
EXP15	Product formation [a]	FTIR	25DMF:	2.5
EXP16	Product formation [a]	FTIR	25DMF:	2.1
EXP17	Product formation [a]	FTIR	25DMF:	1.9
EXP18	Product formation [a]	FTIR	25DMF:	3.9
EXP19	Product formation [a]	FTIR	25DMF: SO_2:	3.3 4.2
EXP20	Product formation [a]	FTIR	25DMF: SO_2:	3.3 5.8
EXP21	Rate coefficient determination [a]	FTIR	25DMF: E2B: SO_2:	3.2 2.1 5.9

[a] Experiments were performed in the presence of about 2 % CO to scavenge OH radicals, [b] FTIR was used only to determine initial reactant concentrations.

B. Rate coefficient calculation

Table S2 Summary of the results from the relative kinetic experiments (EXP1-EXP3, EXP21).

Experiment	Reference	Instrumentation	Rate coefficient ratio	$k \times 10^{16}$/ cm^3 molecule^{-1} s^{-1}
EXP1	*E2*-Butene	FTIR	1.34 ± 0.20	2.7 ± 0.8 [a]
	E2-Butene	PTR-MS	1.74 ± 0.09	3.5 ± 0.9 [a]
	Cyclohexene	PTR-MS	3.91 ± 0.47	3.0 ± 0.6 [a]
EXP2	*E2*-Butene	FTIR	1.69 ± 0.26	3.4 ± 1.0 [a]
	E2-Butene	PTR-MS	1.70 ± 0.08	3.4 ± 0.9 [a]
	Cyclohexene	PTR-MS	4.15 ± 0.61	3.2 ± 0.7 [a]
EXP3	*E2*-Butene	PTR-MS	1.47 ± 0.10	2.9 ± 0.8 [a]
	Cyclohexene	PTR-MS	4.03 ± 0.26	3.1 ± 0.5 [a]
EXP21	*E2*-Butene	FTIR	1.89 ± 0.14	3.8 ± 1.0 [a]
			average	**3.3 ± 1.0 [b]**

[a] The error (2σ) consists of combination of the statistical uncertainty derived from regression analysis and the uncertainty of k_{ref}. [b] The final rate coefficient represents the mean weighted by the errors resulting from regression analysis. The associated error represents a preferred expanded uncertainty of 30 %.

C. Calculation of the OH yield α

OH radicals formed from the ozonolysis of 2,5-dimethylfuran (25DMF) react, in principle, with any reactive VOC present in the reaction system. However, in the initial phase of the reaction OH will react almost exclusively with 1,3,5-trimethylbenzene (135TMB) and 2,5-dimethylfuran since both are highly reactive towards OH radicals and their concentrations exceed product concentrations by at least one order of magnitude. Accordingly, the OH chemistry is represented reasonably by reactions (R1) – (R3) for the initial phase of the reaction.

$$25DMF + O_3 \longrightarrow \alpha\ OH + products \quad (R1)$$

$$25DMF + OH \longrightarrow products \quad (R2)$$

$$135TMB + OH \longrightarrow products \quad (R3)$$

Consequently, the OH production (P_{OH}) and loss rate (L_{OH}) are given by

$$P_{OH} = \alpha \times k_1 \times [25DMF] \times [O_3] \quad (1)$$

$$L_{OH} = k_2 \times [25DMF] \times [OH] + k_3 \times [135TMB] \times [OH] \quad (2)$$

The linearity of $\ln([135TMB]_0/[135TMB]_t)$ *vs.* time from data collected after one single O_3 injection justifies the assumption of a steady-state OH concentration within statistical uncertainties. It applies Eq. (3).

$$\frac{d[OH]}{dt} = P_{OH} - L_{OH} = 0 \quad (3)$$

Combining Equations (1) – (3) yields an equation which allows to calculate the OH yield α.

$$\alpha = \frac{[OH](k_2[25DMF] + k_3[135TMB])}{k_1[25DMF][O_3]} \quad (4)$$

Since 2,5-dimethylfuran was shown to be highly reactive towards ozone, $[O_3]$ is rather low during the experiments. As a consequence, the quantification by FTIR becomes inaccurate. Yet, Eq. (4) can be rewritten as

$$\alpha = \frac{[OH]\left(k_2[25DMF] + k_3[135TMB]\right)}{\beta k'[25DMF]} \tag{5}$$

where *k*' represents the pseudo-first order loss of 2,5-dimethylfuran observed in the experiment after a single O_3 injection. Since *k*' represents the overall loss rate due to both O_3 and OH reaction, a correction factor β must be included, which represents the fraction of loss due to the ozonolysis reaction. The correction factor β is derived from a plot of $\ln([25DMF]_0/[25DMF]_t)$ *vs.* $\ln([135TMB]_0/[135TMB]_t)$. Exemplary plots used for the calculation of α are shown below (Fig. S1).

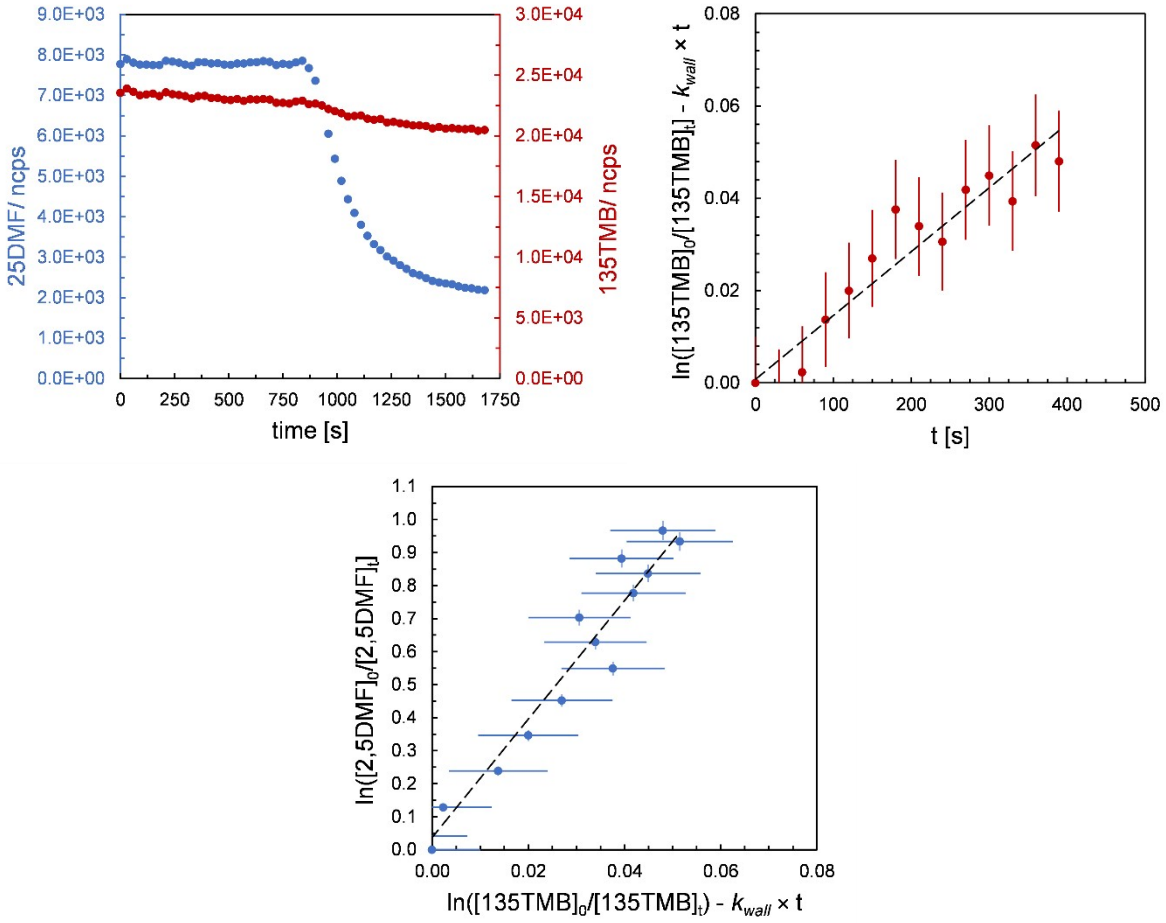

Fig. S1 Upper left: Time profile of 2,5-dimethylfuran (25DMF) and 1,3,5-trimethylbenzene (135TMB) recorded with the PTR-ToF-MS in E11. Upper right: Logarithmic plot of 135TMB after injection of O_3. Lower panel: Plot of 25DMF vs. 135TMB used for the calculation of β.

D. Quantification

1. Absorption cross section determination

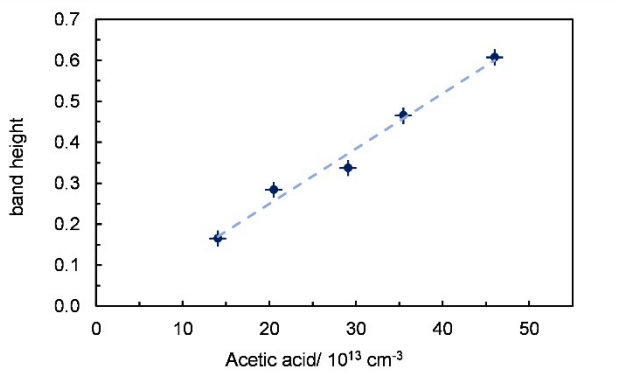

Fig. S3 Correlation between the height of the absorption band at 1177 cm^{-1} and the concentration of acetic acid (at an optical path length of 51.0 m).

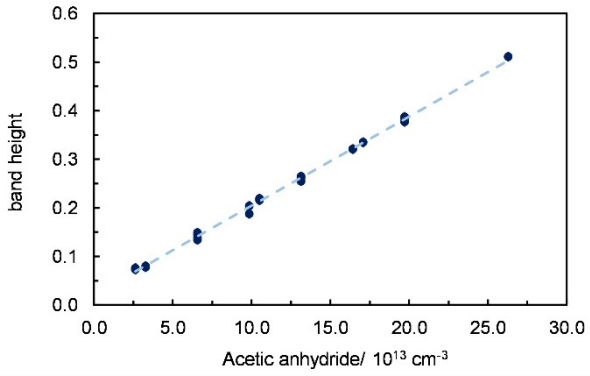

Fig. S3 Correlation between the height of the absorption band at 1778 cm^{-1} and the concentration of acetic anhydride (at an optical path length of 51.0 m).

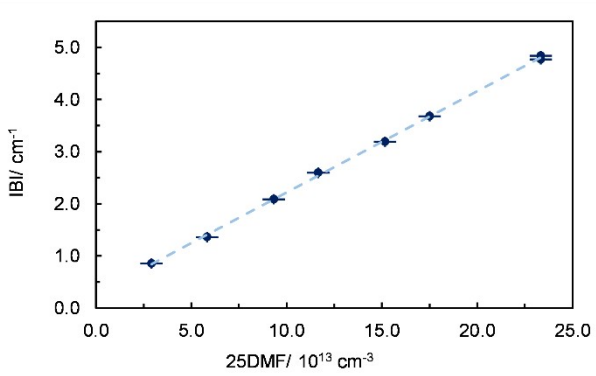

Fig. S4 Correlation between the integrated band intensity (IBI) in the range 1060 – 880 cm^{-1} and the concentration of 2,5-dimethylfuran (at an optical path length of 51.0 m).

2. Quantification of ketene (CH_2=C=O)

Information on the quantification of gaseous ketene were, to the best of our knowledge, published in four studies.[1-4] Two of them reported infrared absorption cross sections[1,2] whereas the other two provided quantitative IR spectra.[3,4]

Tuazon et al.[2] estimated a value of 8.5 × 10^{-18} cm^2 $molecule^{-1}$ (base 10) for the P-branch maximum at 2151.8 cm^{-1} based on the printed spectrum of Halverson and Williams[3]. The assignment is probably a typo since the peak maximum at about 2152 cm^{-1} does correspond clearly to the Q-branch in the published spectrum as well as in a reference spectrum from our laboratory (Fig. S5). Following the procedure of Tuazon et al.[2] we derived cross sections of about 7.8 × 10^{-19} and 9.0 × 10^{-19} cm^2 $molecule^{-1}$ (base 10) for the P-branch and R-branch maximum, respectively. Being estimated from a printed spectrum published back in 1947, these values exhibit significant uncertainty. However, we estimate the error based on deriving a value for the transmission is < 15 %. Since Tuazon et al.[2] rely on the same data we do not see any other conclusion than assuming a typo in the previous study, which stated a ten times larger value.

Applying the same methodology to the printed quantitative IR spectrum of Wallington et al.[4], we derive absolute cross sections of about 7.6 × 10^{-19} and 1.0 × 10^{-18} cm^2 $molecule^{-1}$ (base 10) for the P-branch and R-branch maximum, respectively. Accordingly, both reported IR spectra yield nearly the same absolute cross sections for the R-branch maximum (2164 cm^{-1}) considering the uncertainty from estimating the transmission from a printed spectrum. In the case of the P-branch maximum (2137 cm^{-1}), the estimated values are identical.

The absolute cross section of Hatakeyama et al.[1] (for the R-branch maximum at 2164 cm^{-1}) is about 40 % larger than our estimation from the spectrum of Halverson and Williams[3]. Since both published IR spectra yielded consistent values, it appears that Hatakeyama et al.[1] might have overestimated the ketene concentration. In the absence of additional data, we combined our estimated cross sections and used an average value of 7.7 × 10^{-19} cm^2 $molecule^{-}$

[1] (base 10) for the P-branch maximum at 2137 cm^{-1}. However, we prefer to assign an accuracy error of about 20 %.

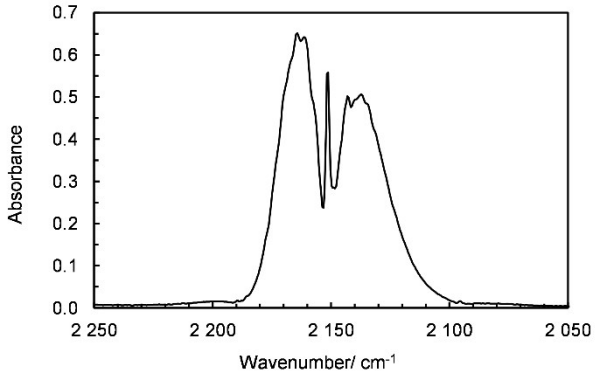

Fig. S5 Reference spectrum of gas-phase ketene showing the main absorption structure.

3. Cross sections

Table S3 Absolute and integrated absorption cross sections (base 10) used for the quantification via FTIR spectroscopy.

Species	Range / cm^{-1}	Integrated cross section / cm $molecule^{-1}$	Absolute cross section / cm^2 $molecule^{-1}$	Reference
Acetic acid	1177		$(2.6 \pm 0.3) \times 10^{-19}$	a
Acetic anhydride	1778		$(3.6 \pm 0.2) \times 10^{-19}$	a
2,5-Dimethylfuran	1060–880	$(3.8 \pm 0.2) \times 10^{-18}$		a
Formaldehyde	1820–1660	$(5.4 \pm 0.3) \times 10^{-18}$		b
Glyoxal	2940–2724	$(7.2 \pm 0.3) \times 10^{-18}$		5
Ketene	2137		7.7×10^{-19}	c
Methyl glyoxal	1880–1600	$(1.31 \pm 0.02) \times 10^{-17}$		6
Methyl hydroperoxide	2961		$(1.09 \pm 0.07) \times 10^{-19}$	b

[a] Determined within this work, [b] Wuppertal laboratory database, [c] see text above.

E. Time profiles and product yield determination

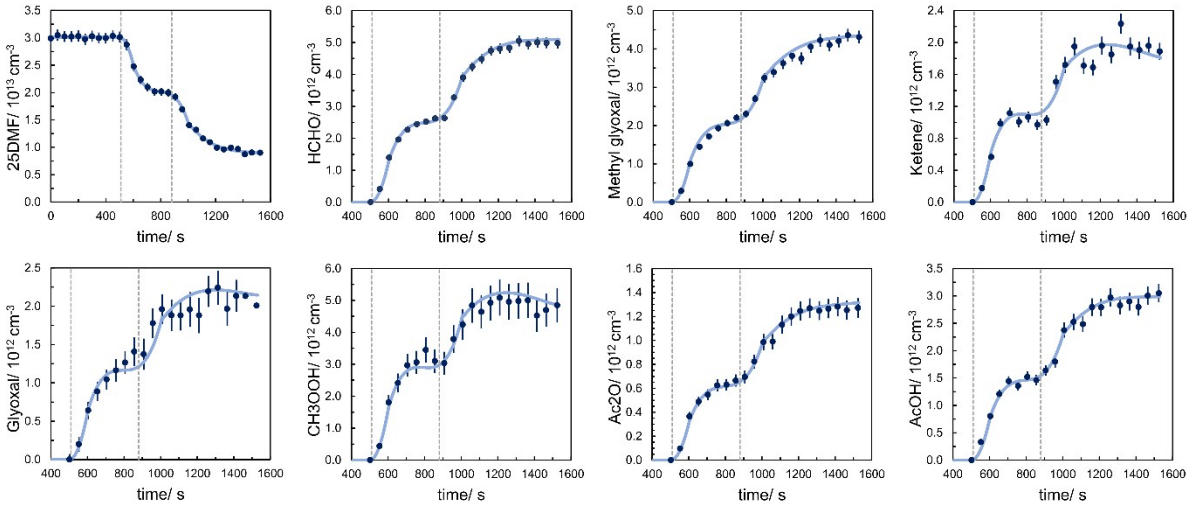

Fig. S6 Concentration-time profiles of quantified species in EXP12. Dark blue dots represent measured data (FTIR) together with the respective statistical uncertainty (2σ). The light blue lines represent the modelled time profiles (best-fit) considering a constant formation yield and a first-order wall loss. The vertical dotted lines mark the respective start of O_3 addition for a period of about 1 min.

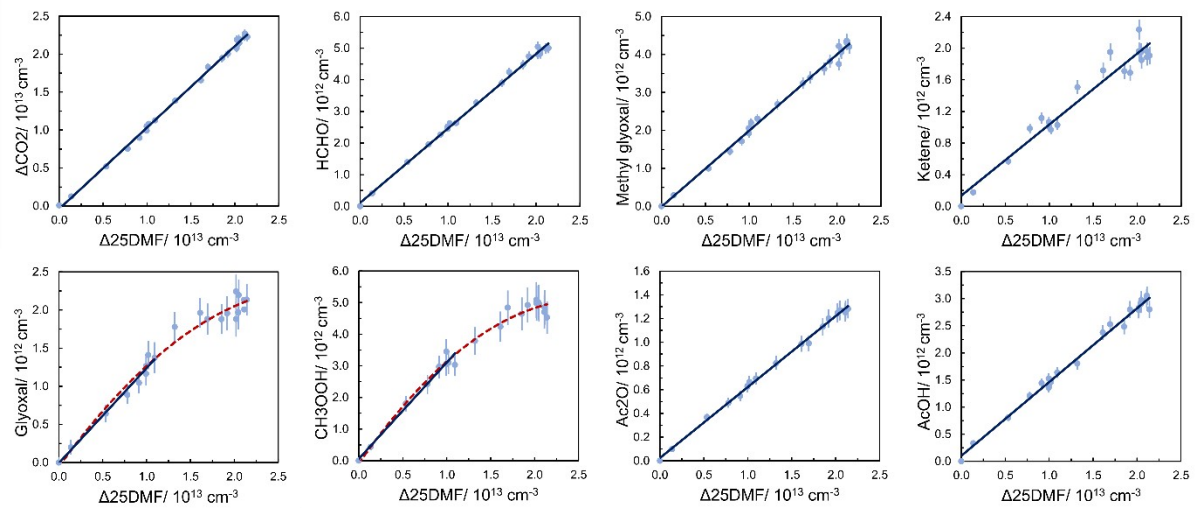

Fig. S7 Yield plots of quantified species in EXP12. Light blue dots represent measured data (FTIR) together with the respective statistical uncertainty (2σ). The solid blue lines represent the linear fit obtained through regression analysis. The dotted red lines represent polynomial functions to aid visual inspection of the non-linearity.

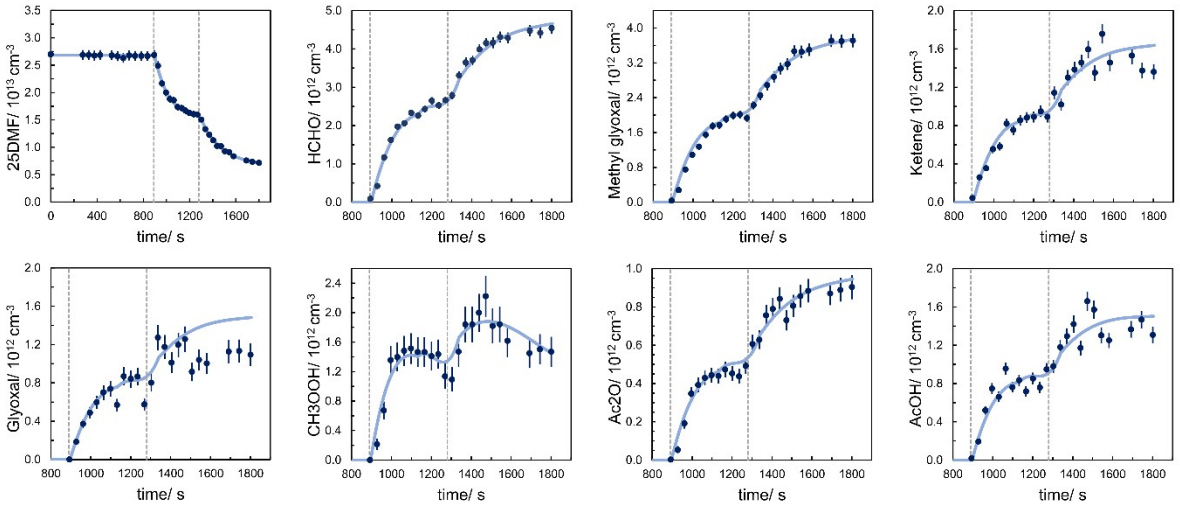

Fig. S8 Concentration-time profiles of quantified species in EXP14. Dark blue dots represent measured data (FTIR) together with the respective statistical uncertainty (2σ). The light blue lines represent the modelled time profiles (best-fit) considering a constant formation yield and a first-order wall loss. The vertical dotted lines mark the respective start of O_3 addition for a period of about 1 min.

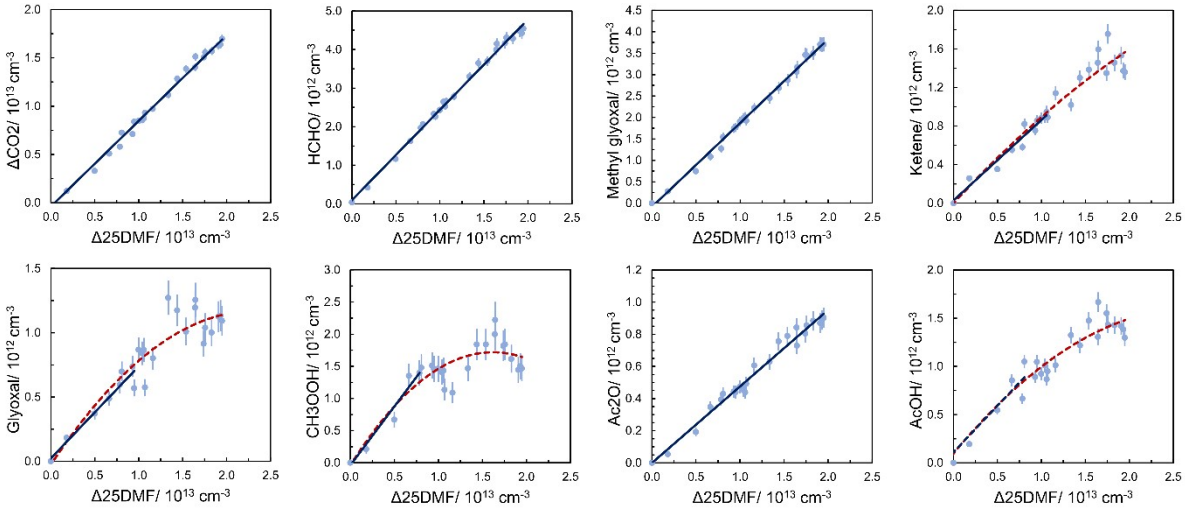

Fig. S9 Yield plots of quantified species in EXP14. Light blue dots represent measured data (FTIR) together with the respective statistical uncertainty (2σ). The solid blue lines represent the linear fit obtained through regression analysis. The dotted red lines represent polynomial functions to aid visual inspection of the non-linearity.

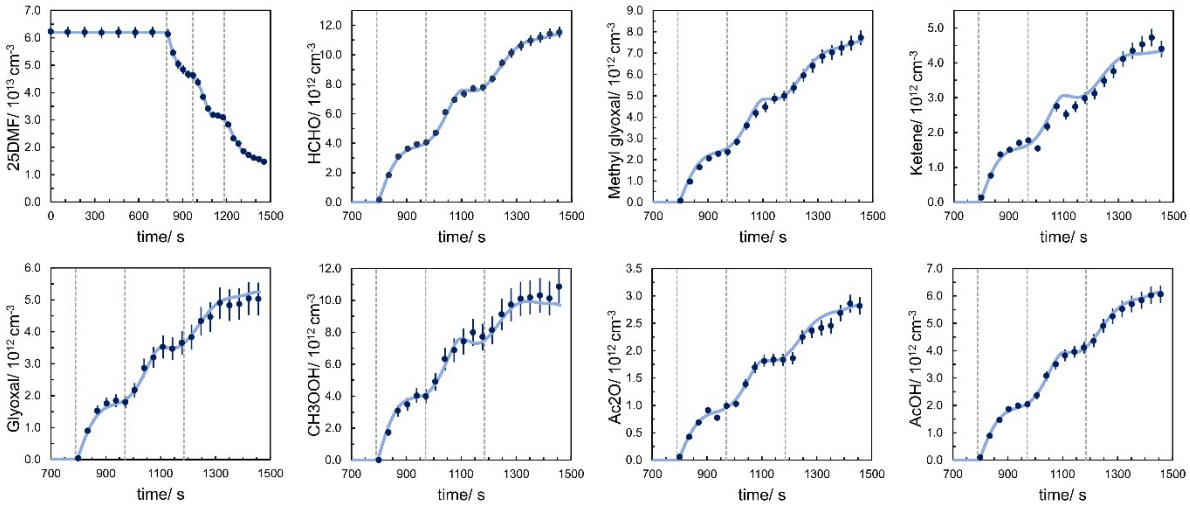

Fig. S10 Concentration-time profiles of quantified species in EXP15. Dark blue dots represent measured data (FTIR) together with the respective statistical uncertainty (2σ). The light blue lines represent the modelled time profiles (best-fit) considering a constant formation yield and a first-order wall loss. The vertical dotted lines mark the respective start of O_3 addition for a period of about 1 min.

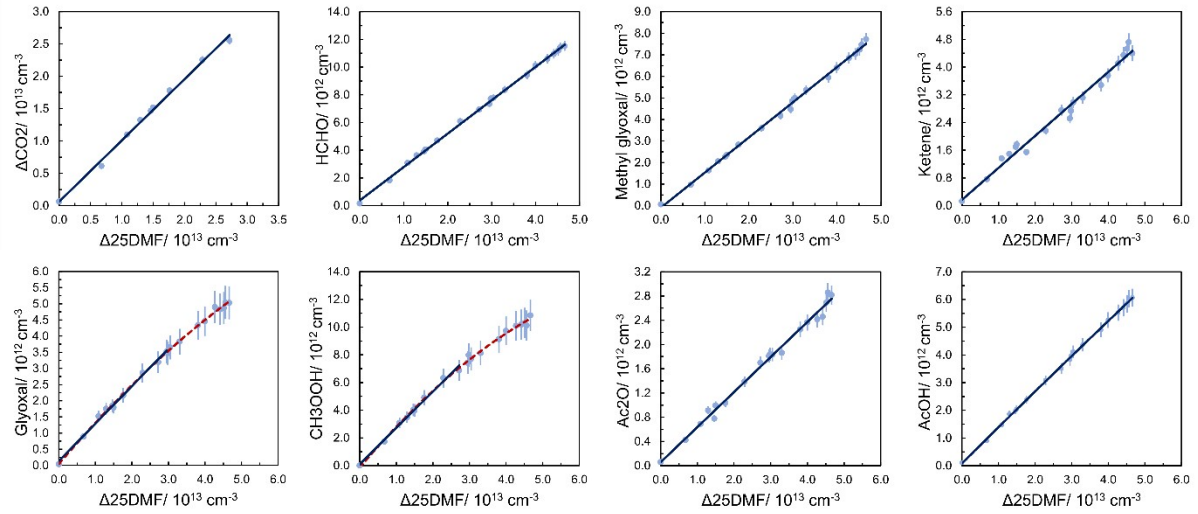

Fig. S11 Yield plots of quantified species in EXP15. Light blue dots represent measured data (FTIR) together with the respective statistical uncertainty (2σ). The solid blue lines represent the linear fit obtained through regression analysis. The dotted red lines represent polynomial functions to aid visual inspection of the non-linearity.

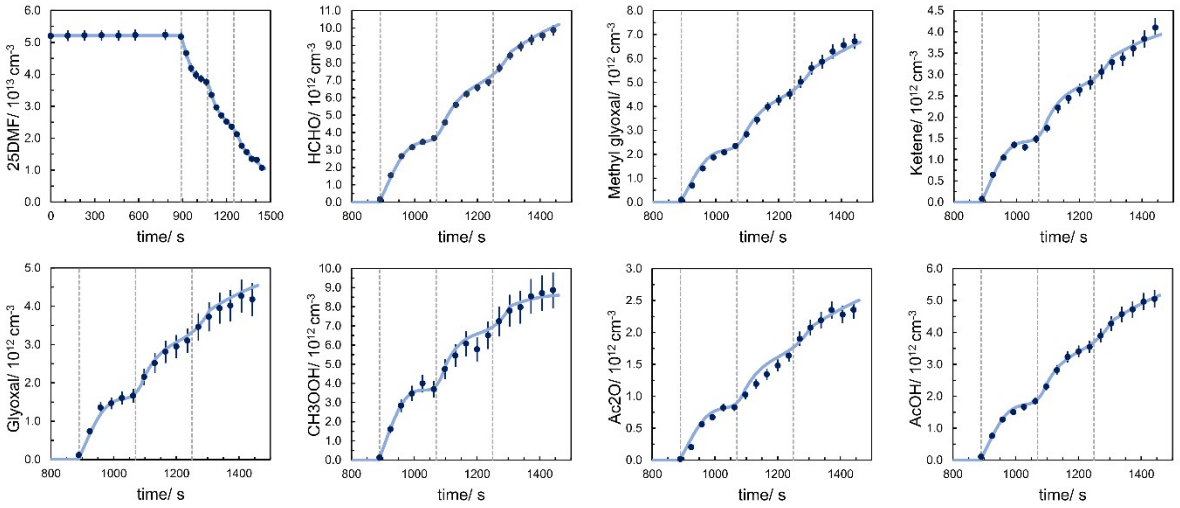

Fig. S12 Concentration-time profiles of quantified species in EXP16. Dark blue dots represent measured data (FTIR) together with the respective statistical uncertainty (2σ). The light blue lines represent the modelled time profiles (best-fit) considering a constant formation yield and a first-order wall loss. The vertical dotted lines mark the respective start of O_3 addition for a period of about 1 min.

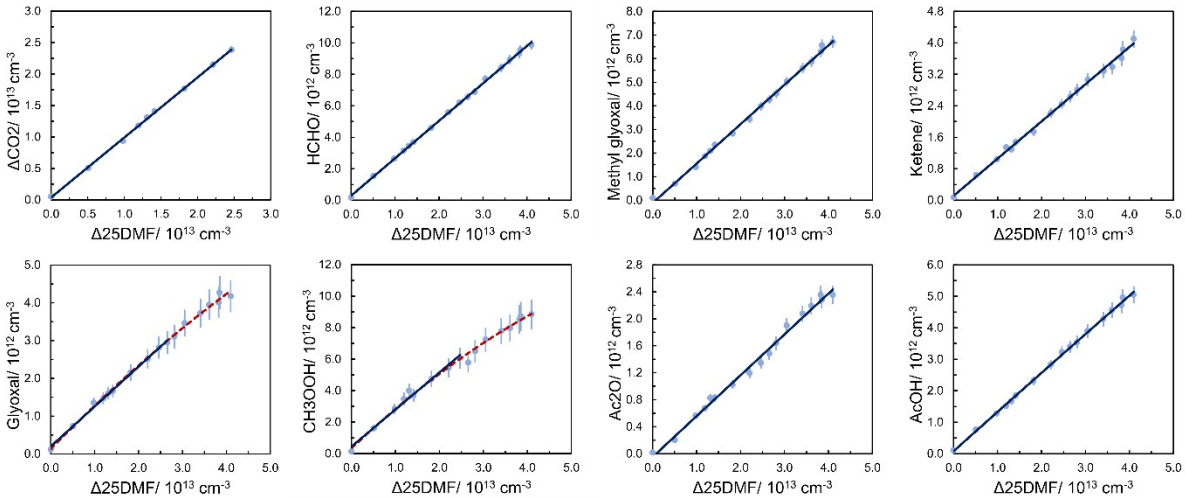

Fig. S13 Yield plots of quantified species in EXP16. Light blue dots represent measured data (FTIR) together with the respective statistical uncertainty (2σ). The solid blue lines represent the linear fit obtained through regression analysis. The dotted red lines represent polynomial functions to aid visual inspection of the non-linearity.

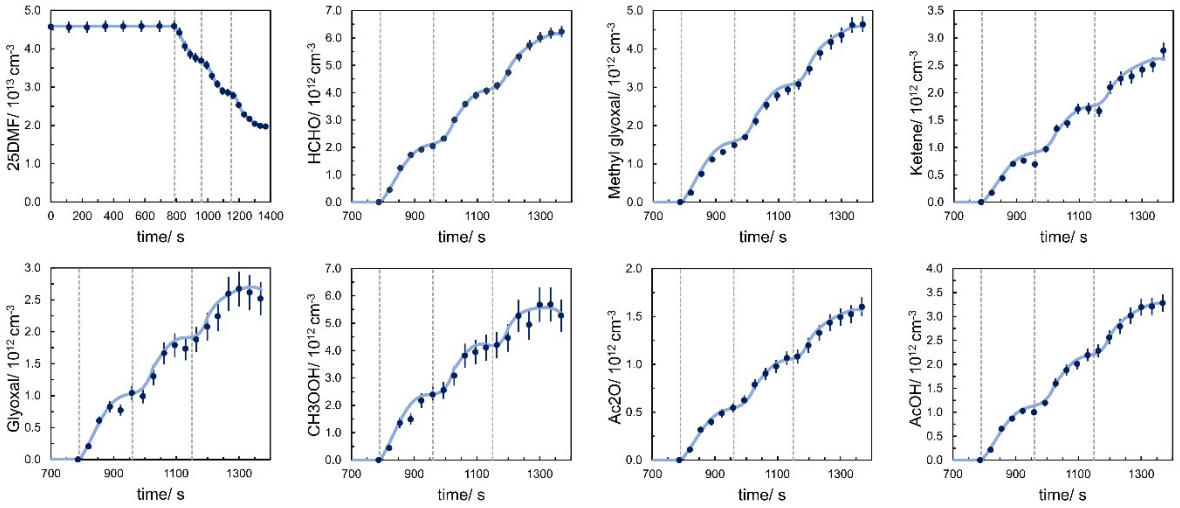

Fig. S14 Concentration-time profiles of quantified species in EXP17. Dark blue dots represent measured data (FTIR) together with the respective statistical uncertainty (2σ). The light blue lines represent the modelled time profiles (best-fit) considering a constant formation yield and a first-order wall loss. The vertical dotted lines mark the respective start of O_3 addition for a period of about 1 min.

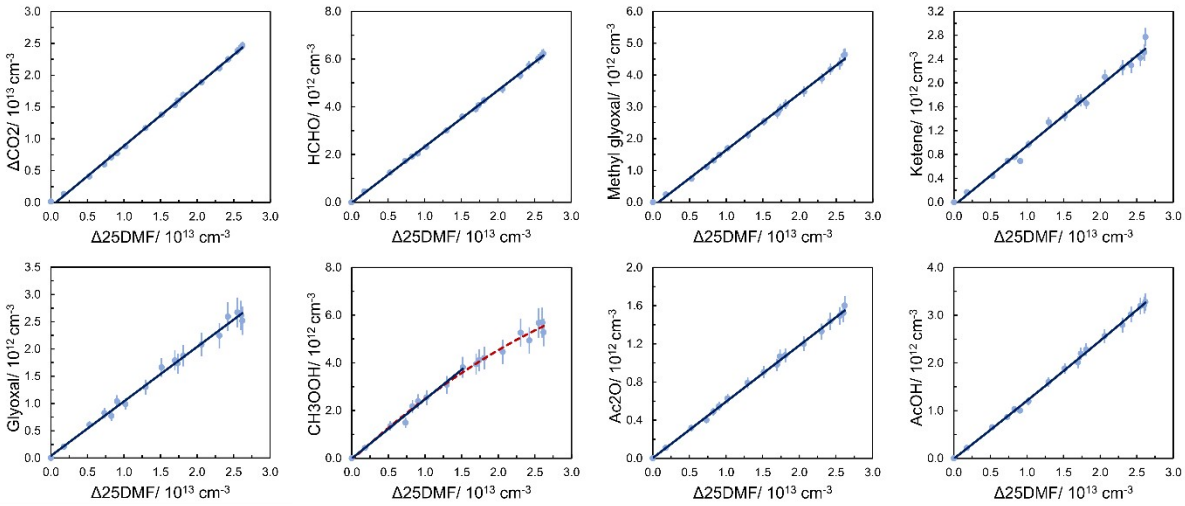

Fig. S15 Yield plots of quantified species in EXP17. Light blue dots represent measured data (FTIR) together with the respective statistical uncertainty (2σ). The solid blue lines represent the linear fit obtained through regression analysis. The dotted red lines represent polynomial functions to aid visual inspection of the non-linearity.

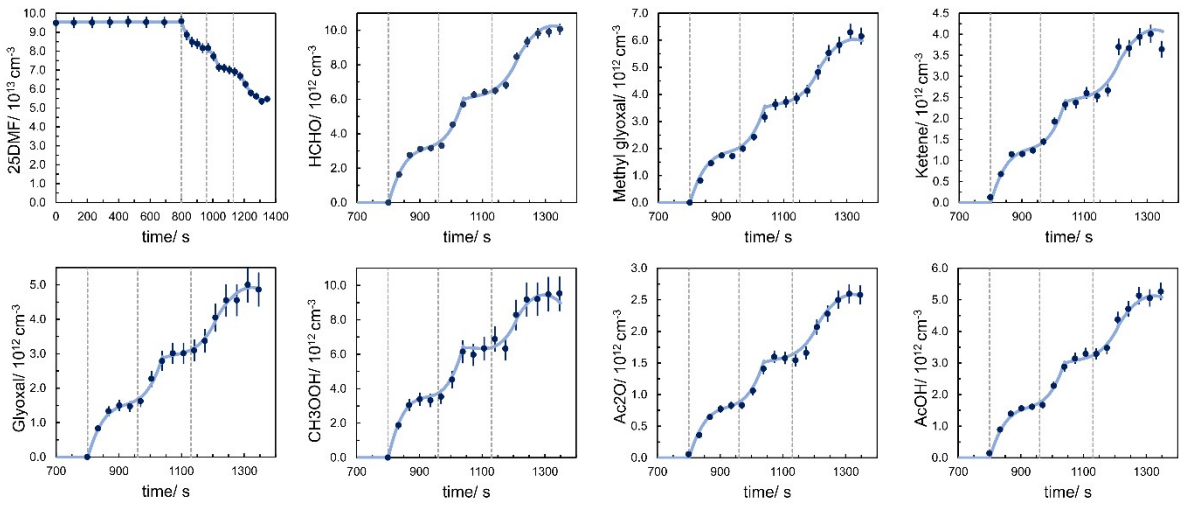

Fig. S16 Concentration-time profiles of quantified species in EXP18. Dark blue dots represent measured data (FTIR) together with the respective statistical uncertainty (2σ). The light blue lines represent the modelled time profiles (best-fit) considering a constant formation yield and a first-order wall loss. The vertical dotted lines mark the respective start of O_3 addition for a period of about 1 min.

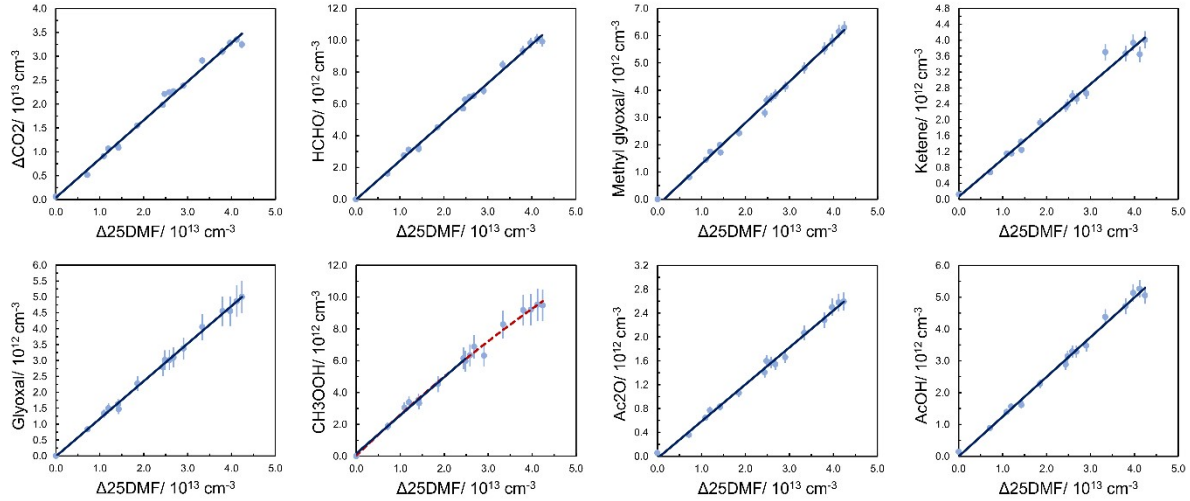

Fig. S17 Yield plots of quantified species in EXP18. Light blue dots represent measured data (FTIR) together with the respective statistical uncertainty (2σ). The solid blue lines represent the linear fit obtained through regression analysis. The dotted red lines represent polynomial functions to aid visual inspection of the non-linearity.

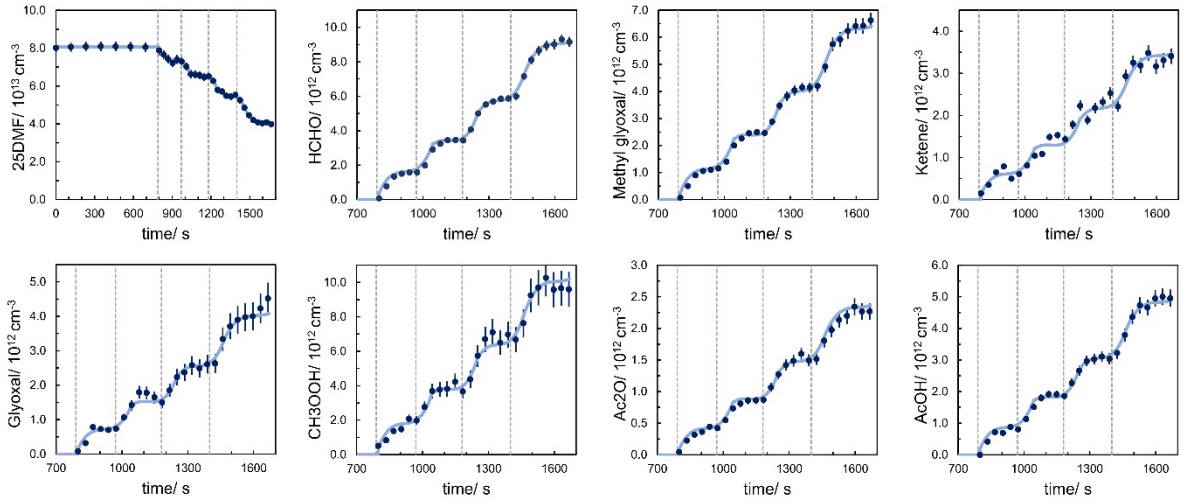

Fig. S18 Concentration-time profiles of quantified species in EXP19. Dark blue dots represent measured data (FTIR) together with the respective statistical uncertainty (2σ). The light blue lines represent the modelled time profiles (best-fit) considering a constant formation yield and a first-order wall loss. The vertical dotted lines mark the respective start of O_3 addition for a period of about 1 min.

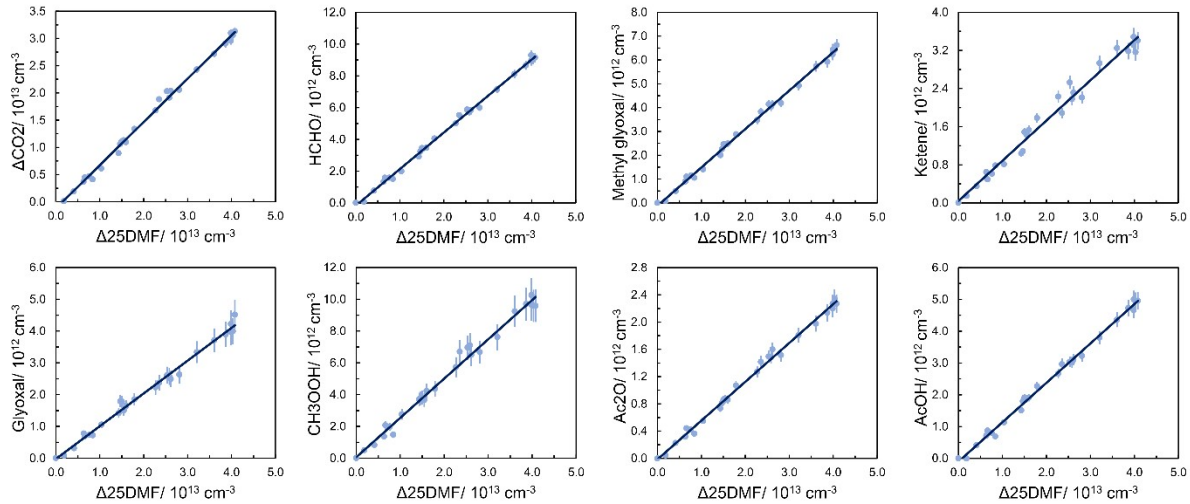

Fig. S19 Yield plots of quantified species in EXP19. Dark blue dots represent measured data (FTIR) together with the respective statistical uncertainty (2σ). The solid blue lines represent the linear fit obtained through regression analysis.

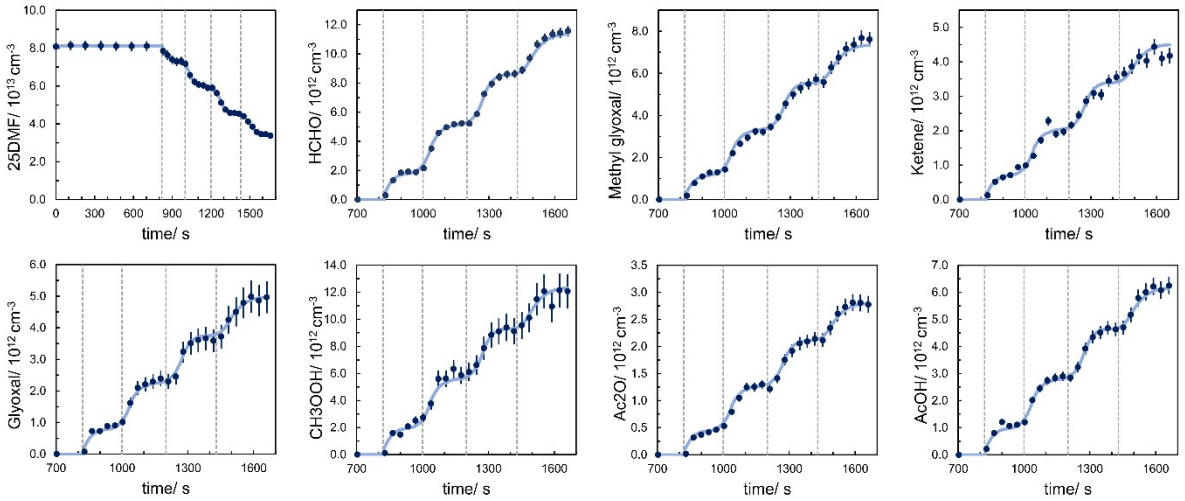

Fig. S20 Concentration-time profiles of quantified species in EXP20. Dark blue dots represent measured data (FTIR) together with the respective statistical uncertainty (2σ). The light blue lines represent the modelled time profiles (best-fit) considering a constant formation yield and a first-order wall loss. The vertical dotted lines mark the respective start of O_3 addition for a period of about 1 min.

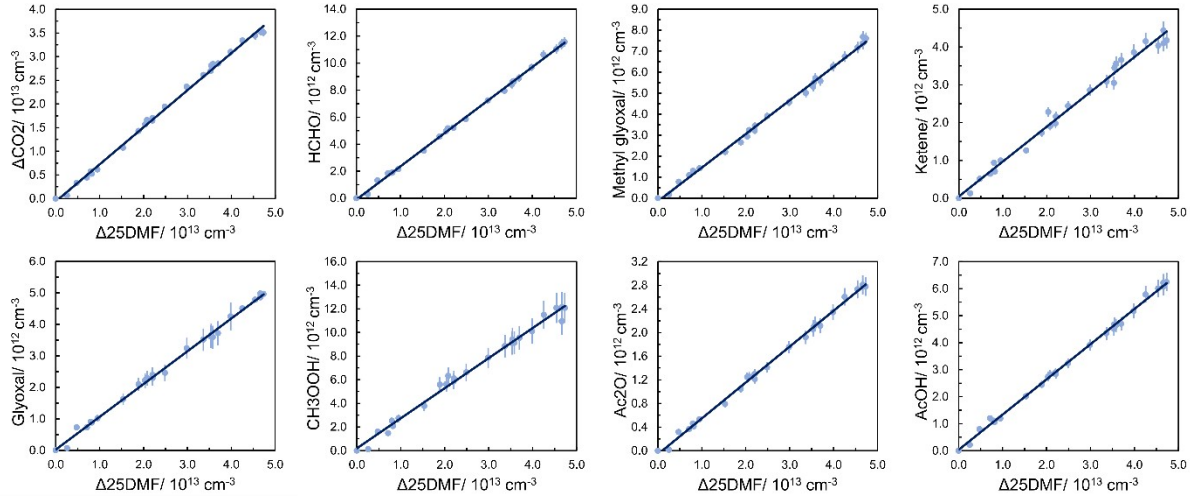

Fig. S21 Yield plots of quantified species in EXP20. Light blue dots represent measured data (FTIR) together with the respective statistical uncertainty (2σ). The solid blue lines represent the linear fit obtained through regression analysis.

F. Modelling

In order to check if we are able to explain non-linearity observed in some yield plots by assuming a unimolecular wall loss, we simulated the time profiles using a simplified modelling approach[7], which is based on the Euler-Cauchy method. In practice, concentration changes

Δc are calculated for each time interval using an Excel® spreadsheet in order to obtain time profiles for each species. Given its purpose, the mechanism behind the model is a simplified reaction scheme assuming that a product P_n is formed by the ozonolysis reaction with a constant formation yield γ_n and potentially lost by an irreversible first-order wall loss:

$$25DMF + O_3 \rightarrow \gamma_1 P_1 + \gamma_2 P_2 + \gamma_3 P_3 + \ldots \quad \text{(R4)}$$

$$P_1 + \text{wall} \rightarrow \text{loss} \quad \text{(R5)}$$

$$P_2 + \text{wall} \rightarrow \text{loss} \quad \text{(R6)}$$

$$P_3 + \text{wall} \rightarrow \text{loss} \quad \text{(R7)}$$

Both, the formation yield γ_n and the wall loss rate coefficient $k_{wall,n}$ for the species P_n are included as parameters, which are varied until a match between the experimental data and the simulated time profile is achieved if possible. This procedure relies on the assumption that the time profile of a product is dominated by the formation immediately after the O_3 injection whereas a potential wall loss dominates once the reaction rate slows down significantly. Since O_3 is almost entirely consumed during the reaction and up to four O_3 injections were necessary in the experiments, we cannot use a steady-state oxidant concentration for the calculations of Δc. Instead, the time profile of 2,5-dimethylfuran is fitted by second or third order polynomials chosen to reproduce the experimental values over a certain reaction time, i.e. between the O_3 injections. The parameters used to describe the time profiles of products are summarized in Tab. S4.

Table S4 Product yields obtained through regression analysis and yield and wall loss parameters obtained through modelling for all product study experiments (EXP12 – EXP20).

Experiment		HCHO	Methyl glyoxal	Ketene	Glyoxal	CH_3OOH	Ac2O	Acetic acid
EXP12	Yield [a]	23.5 ± 0.6 %	20.0 ± 0.7 %	9.4 ± 1.1 %	12.4 ± 1.4 %	30.5 ± 3.6 %	6.0 ± 0.2 %	12.9 ± 0.4 %
	Yield [b]	25.5 %	20.5 %	12.2 %	12.4 %	32.0 %	6.2 %	15.0 %
	k_{wall} [b]	8×10^{-5} s^{-1}	0 s^{-1}	2×10^{-4} s^{-1}	3×10^{-4} s^{-1}	5×10^{-4} s^{-1}	0 s^{-1}	5×10^{-5} s^{-1}
EXP13	Yield [a]	23.0 ± 0.4 %	19.1 ± 0.4 %	7.5 ± 0.5 %	10.0 ± 0.7 %	23.8 ± 4.2 %	5.7 ± 0.2 %	12.5 ± 0.5 %
	Yield [b]	24.0 %	18.0 %	10.0 %	11.0 %	24.0 %	5.8 %	14.0 %
	k_{wall} [b]	5×10^{-5} s^{-1}	0 s^{-1}	2×10^{-4} s^{-1}	5×10^{-4} s^{-1}	1.1×10^{-3} s^{-1}	0 s^{-1}	1.2×10^{-4} s^{-1}
EXP14	Yield [a]	24.0 ± 0.6 %	19.6 ± 0.6 %	8.3 ± 1.0 %	7.1 ± 1.2 %	18.3 ± 3.8 %	4.8 ± 0.3 %	10.3 ± 4.2 %
	Yield [b]	24.0 %	19.0 %	9.0 %	8.0 %	19.0 %	4.8 %	9.0 %
	k_{wall} [b]	5×10^{-5} s^{-1}	0 s^{-1}	1×10^{-4} s^{-1}	1×10^{-4} s^{-1}	1.7×10^{-3} s^{-1}	0 s^{-1}	2×10^{-4} s^{-1}
EXP15	Yield [a]	24.1 ± 0.4 %	16.3 ± 0.4 %	9.2 ± 0.6 %	11.2 ± 0.6 %	26.2 ± 1.8 %	5.8 ± 0.2 %	12.8 ± 0.2 %
	Yield [b]	26.0 %	16.0 %	11.0 %	12.0 %	29.0 %	6.0 %	13.0 %
	k_{wall} [b]	2×10^{-4} s^{-1}	0 s^{-1}	2×10^{-4} s^{-1}	2×10^{-4} s^{-1}	9×10^{-4} s^{-1}	0 s^{-1}	0 s^{-1}
EXP16	Yield [a]	23.8 ± 0.4 %	16.7 ± 0.4 %	9.4 ± 0.3 %	10.3 ± 0.4 %	23.6 ± 2.2 %	6.1 ± 0.2 %	12.3 ± 0.2 %
	Yield [b]	26.0 %	16.0 %	11.0 %	12.0 %	28.0 %	6.0 %	13.0 %
	k_{wall} [b]	2×10^{-4} s^{-1}	0 s^{-1}	2×10^{-4} s^{-1}	3×10^{-4} s^{-1}	8×10^{-4} s^{-1}	0 s^{-1}	8×10^{-5} s^{-1}

EXP17	Yield [a]	23.6 ± 0.4 %	17.7 ± 0.4 %	9.8 ± 0.4 %	10.3 ± 1.2 %	24.8 ± 2.2 %	5.9 ± 0.2 %	12.5 ± 0.2 %
	Yield [b]	23.5 %	17.5 %	10.0 %	12.0 %	28.0 %	6.0 %	12.5 %
	k_{wall} [b]	0 s^{-1}	5 × 10^{-4} s^{-1}	0 s^{-1}	5 × 10^{-4} s^{-1}	8 × 10^{-4} s^{-1}	0 s^{-1}	0 s^{-1}
EXP18	Yield [a]	24.4 ± 0.8 %	15.1 ± 0.6 %	9.4 ± 0.7 %	11.8 ± 0.8 %	23.6 ± 1.8 %	6.2 ± 0.2 %	12.5 ± 0.6 %
	Yield [b]	25.0 %	14.7 %	10.0 %	12.0 %	28.0 %	6.3 %	12.5 %
	k_{wall} [b]	0 s^{-1}	0 s^{-1}	0 s^{-1}	0 s^{-1}	8 × 10^{-4} s^{-1}	0 s^{-1}	0 s^{-1}
EXP19	Yield [a]	23.0 ± 1.0 %	16.2 ± 0.6 %	8.9 ± 0.8 %	11.8 ± 1.6 %	26.3 ± 1.8 %	5.9 ± 0.2 %	12.3 ± 0.6 %
	Yield [b]	22.5 %	15.7 %	8.5 %	10.0 %	25.0 %	5.8 %	12.0 %
	k_{wall} [b]	0 s^{-1}	0 s^{-1}	0 s^{-1}	0 s^{-1}	0 s^{-1}	0 s^{-1}	0 s^{-1}
EXP20	Yield [a]	24.2 ± 0.4 %	15.5 ± 0.4 %	9.6 ± 0.6 %	11.1 ± 0.8 %	25.9 ± 1.2 %	6.0 ± 0.2 %	12.8 ± 0.4 %
	Yield [b]	24.0 %	15.5 %	9.5 %	10.5 %	26.0 %	5.9 %	13.0 %
	k_{wall} [b]	0 s^{-1}	0 s^{-1}	0 s^{-1}	0 s^{-1}	0 s^{-1}	0 s^{-1}	0 s^{-1}

[a] Experimentally determined product yield and the corresponding statistical uncertainty (2σ), [b] parameters obtained through modelling.

G. FTIR spectra

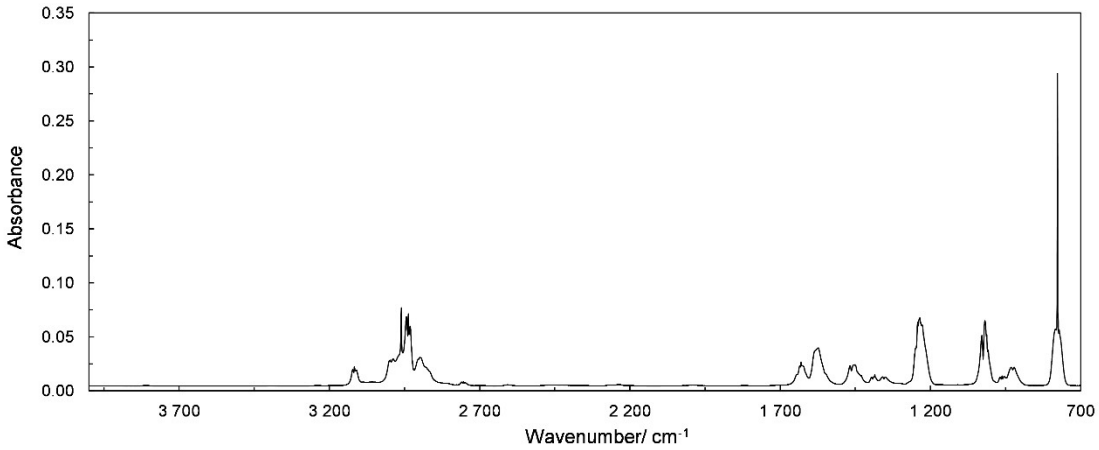

Fig. S22 Reference spectrum of 2,5-dimethylfuran.

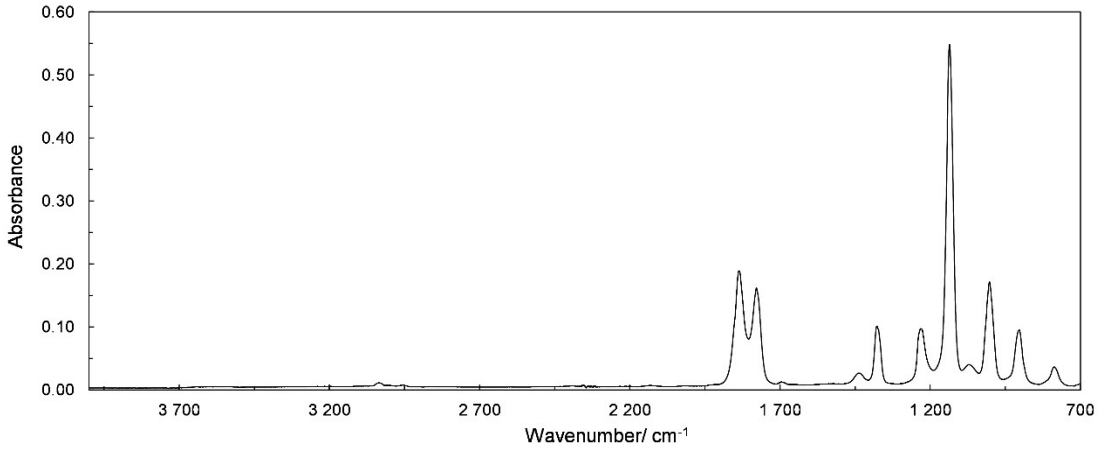

Fig. S23 Reference spectrum of acetic anhydride.

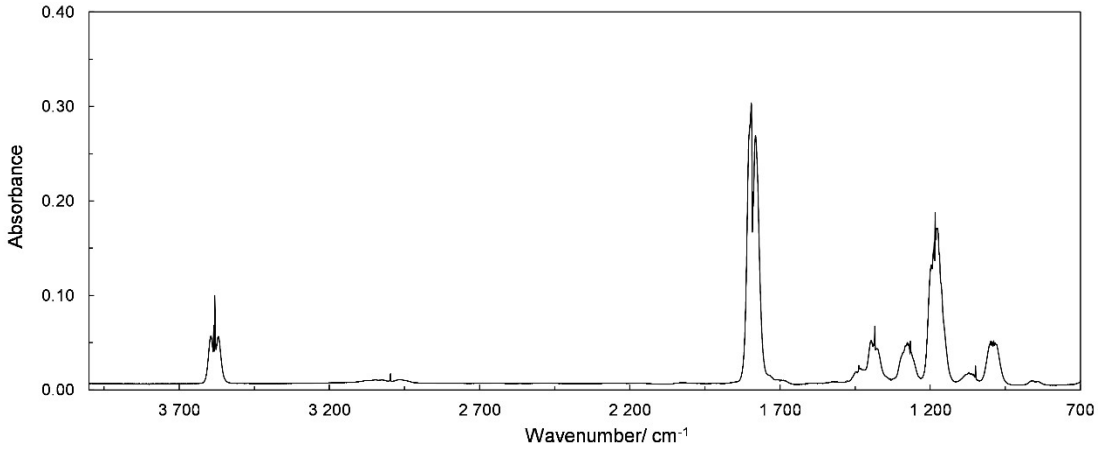

Fig. S24 Reference spectrum of acetic acid.

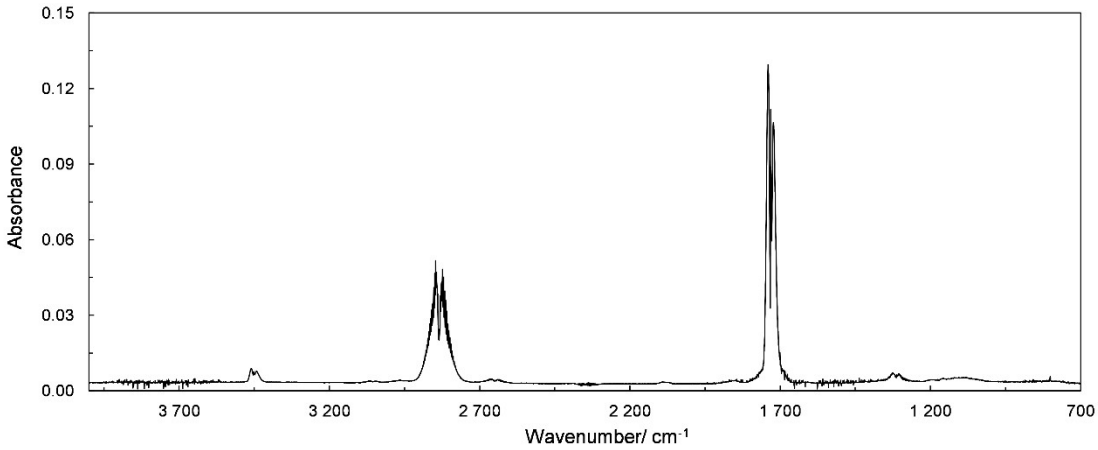

Fig. S25 Reference spectrum of glyoxal.

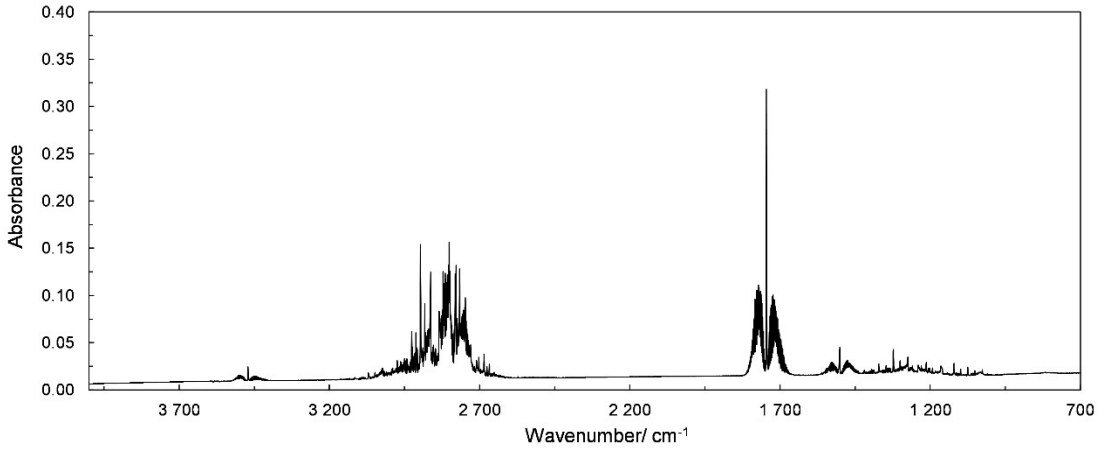

Fig. S26 Reference spectrum of formaldehyde.

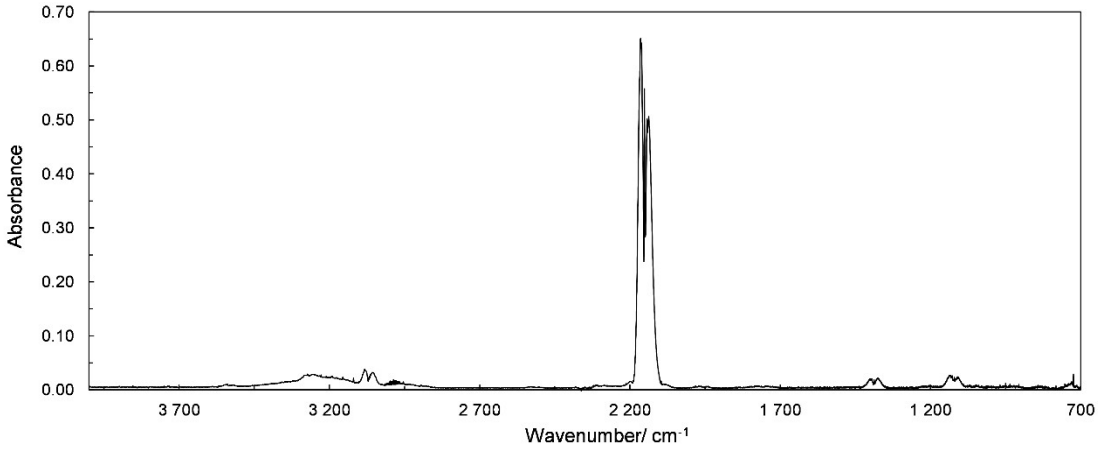

Fig. S27 Reference spectrum of ketene.

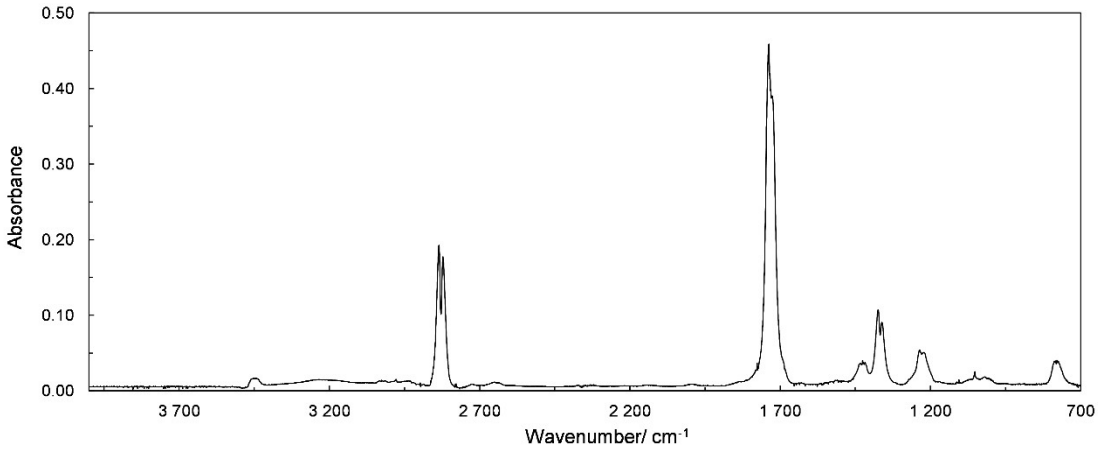

Fig. S28 Reference spectrum of methyl glyoxal.

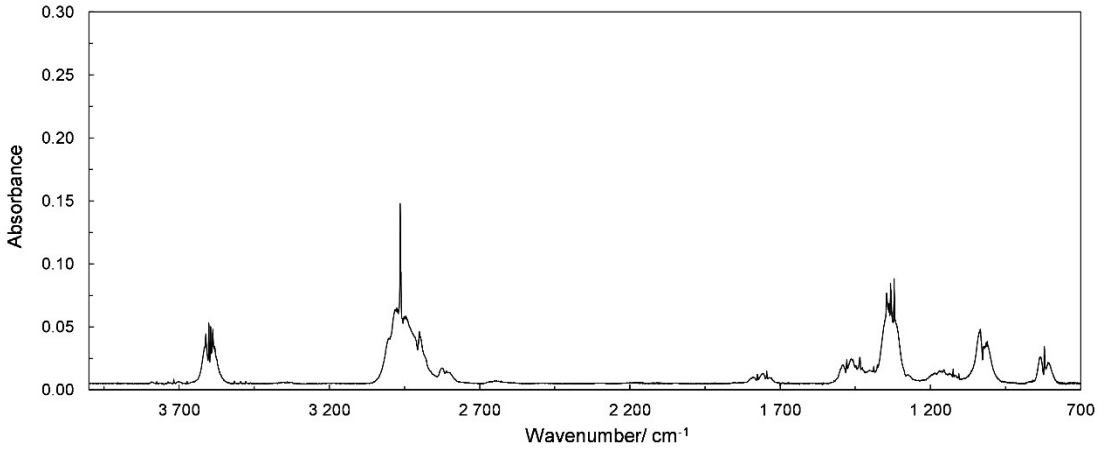

Fig. S29 Reference spectrum of methyl hydroperoxide.

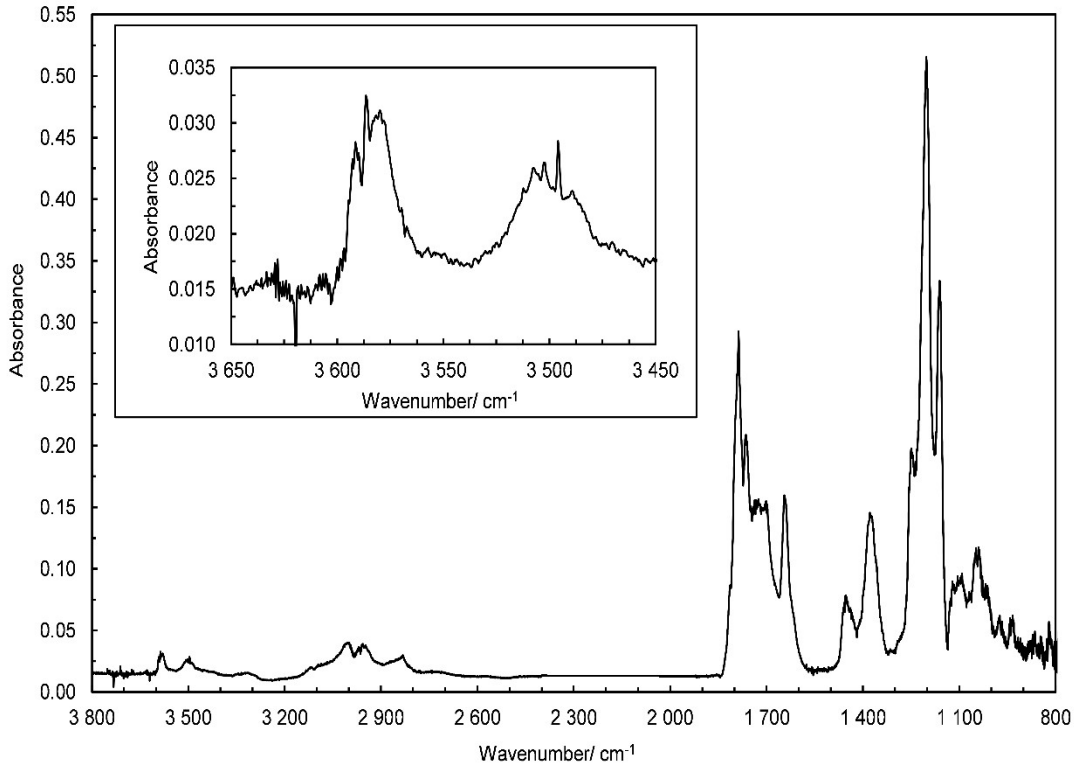

Fig. S30 Residual FTIR spectrum from experiment EXP18. The spectrum was cut in the range 2400 – 1950 cm^{-1} and shifted vertically for readability reasons.

H. Time profiles of PTR-MS data

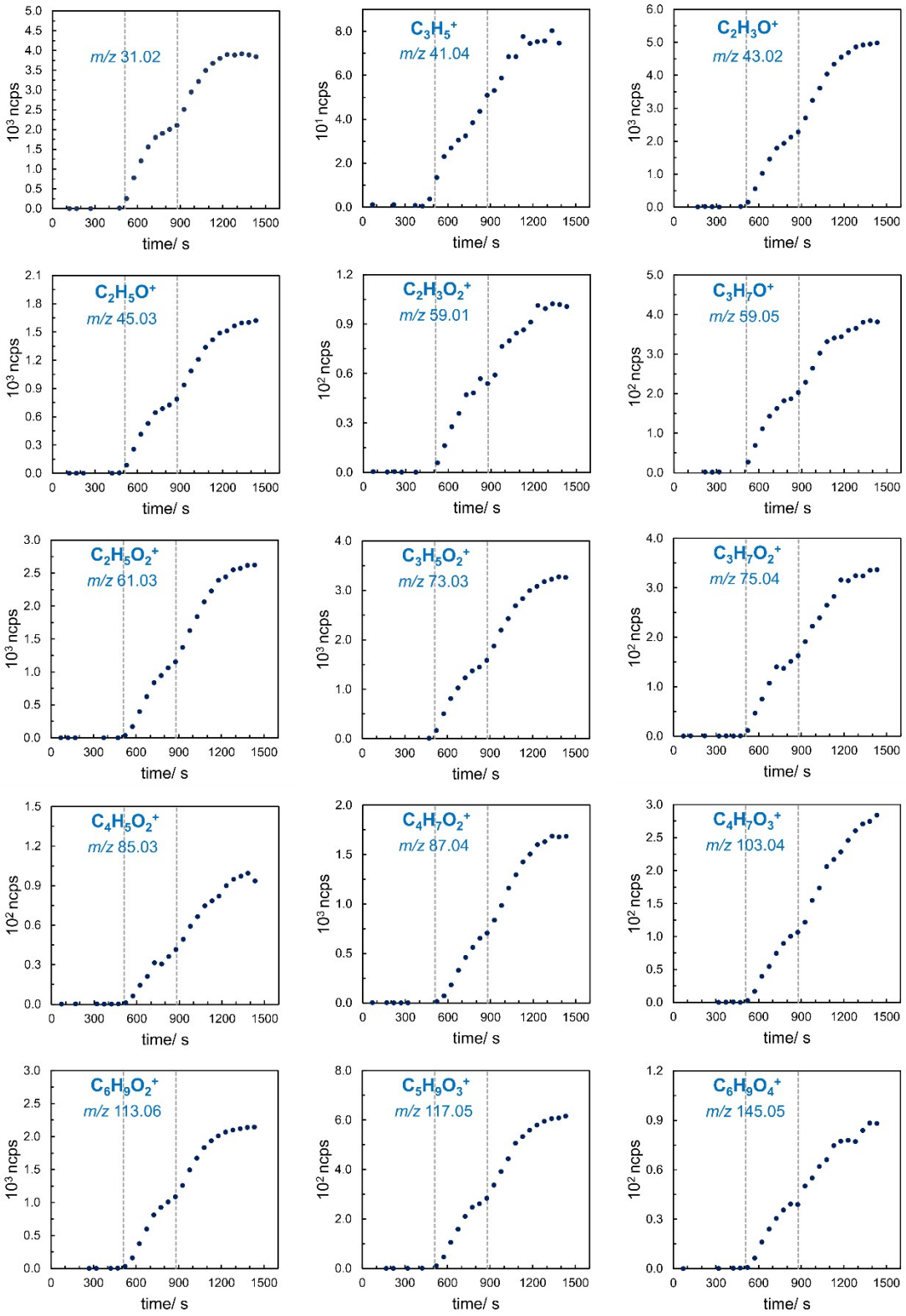

Fig. S31 Time profiles of *m/z* signals of products in EXP12. The vertical dotted lines mark the respective start of O_3 addition for a period of about 1 min.

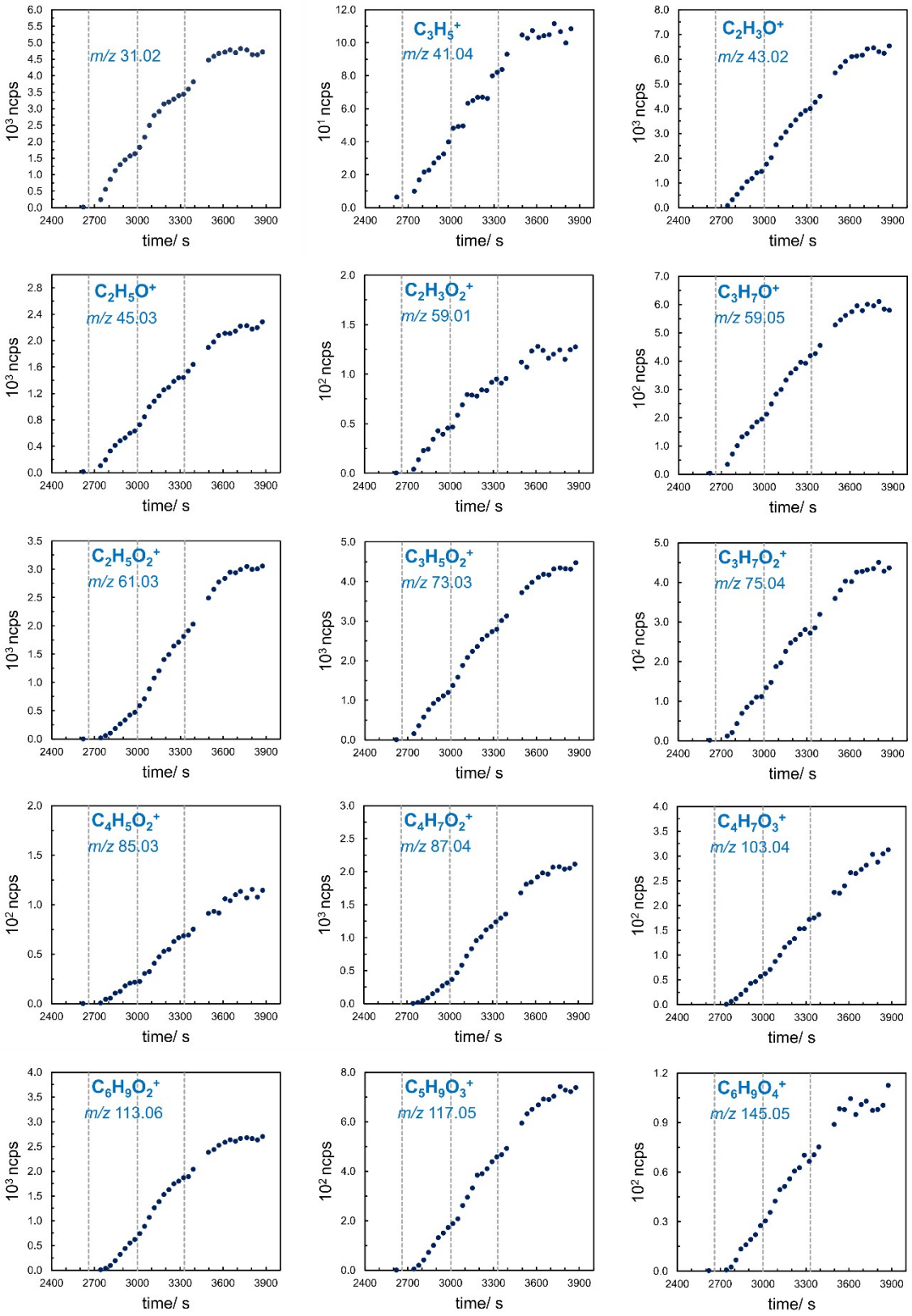

Fig. S32 Time profiles of *m/z* signals of products in EXP13. The vertical dotted lines mark the respective start of O_3 addition for a period of about 1 min.

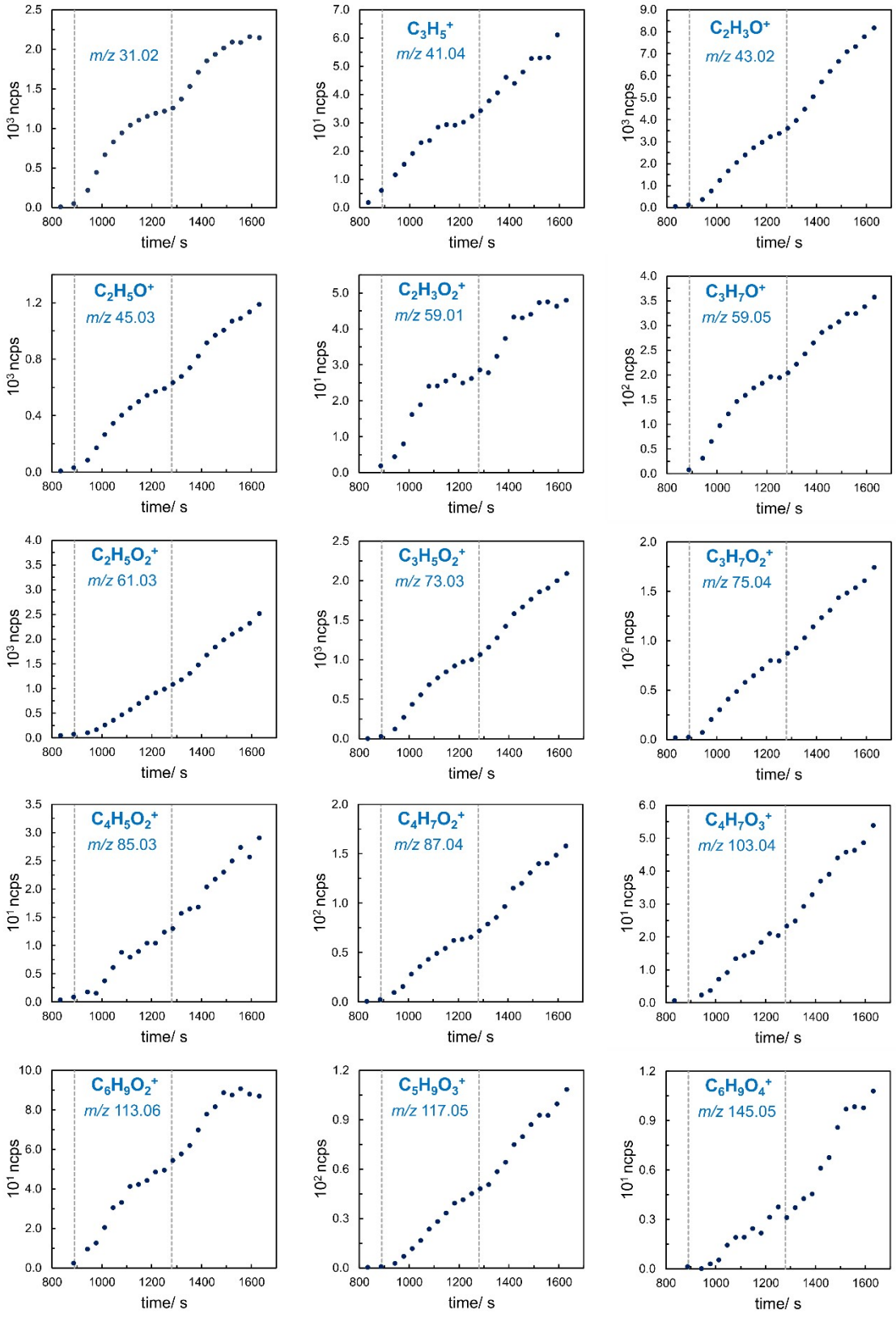

Fig. S33 Time profiles of *m/z* signals of products in EXP14. The vertical dotted lines mark the respective start of O_3 addition for a period of about 1 min.

References

1 S. Hatakeyama, S. Honda, N. Washida, and H. Akimoto, Rate Constants and Mechanism for Reactions of Ketenes with OH Radicals in Air at 299 ± 2 K, *Bull. Chem. Soc. Jpn*., 1985, **58**, 2157–2162.

2 E. C. Tuazon, S. M. Aschmann, J. Arey, and R. Atkinson, Products of the Gas-Phase Reactions of O_3 with a Series of Methyl-Substituted Ethenes, *Environ. Sci. Technol*, 1997, **31**, 3004–3009.

3 F. Halverson, and V. Z. Williams, The Infra-Red Spectrum of Ketene, *J. Chem Phys*., 1947, **15**, 552–559.

4 T. J. Wallington, J. C. Ball, A. M. Straccia, M. D. Hurley, E. W. Kaiser, M. Dill, and W. F. Schneider, Kinetics and Mechanism of the Reaction of Cl Atoms with CH_2CO (Ketene), *Int. J. Chem. Kin*., 1996, **28**, 627–635.

5 R. Volkamer, P. Spietz, J. Burrows, and U. Platt, High-resolution absorption cross-section of glyoxal in the UV–vis and IR spectral ranges, *J. Photochem. Photobiol*., 2005, **172**, 35–46.

6 R. K. Talukdar, L. Zhu, K. J. Feierabend, and J. B. Burkholder, Rate coefficients for the reaction of methylglyoxal (CH_3COCHO) with OH and NO_3 and glyoxal $(HCO)_2$ with NO_3, *Atmos. Chem. Phys*., 2011, **11**, 10837–10851.

7 N. Illmann, R. G. Gibilisco, I. G. Bejan, I. Patroescu-Klotz and P. Wiesen, Atmospheric oxidation of α,β-unsaturated ketones: kinetics and mechanism of the OH radical reaction, Atmos. Chem. Phys., 2021, **21**, 13667–13686.